THE JOURNAL OF PHYSICAL CHEMISTRY LETTERS
A JOURNAL OF THE AMERICAN CHEMICAL SOCIETY

pubs.acs.org/JPCL Letter

DeepBAR: A Fast and Exact Method for Binding Free Energy Computation

Xinqiang Ding and Bin Zhang*

Cite This: J. Phys. Chem. Lett. 2021, 12, 2509−2515 Read Online

ACCESS | Metrics & More | Article Recommendations | Supporting Information

ABSTRACT: The fast and accurate calculation of standard binding free energy has many important applications. Existing methodologies struggle at balancing accuracy and efficiency. We introduce a new method to compute binding free energy using deep generative models and the Bennett acceptance ratio method (DeepBAR). Compared to the rigorous potential of mean force (PMF) approach that requires sampling from intermediate states, DeepBAR is an order-of-magnitude more efficient as demonstrated in a series of host−guest systems. Notably, DeepBAR is exact and does not suffer from approximations for entropic contributions used in methods such as the molecular mechanics energy combined with the generalized Born and surface area continuum solvation (MM/GBSA). We anticipate DeepBAR to be a valuable tool for computing standard binding free energy used in drug design.

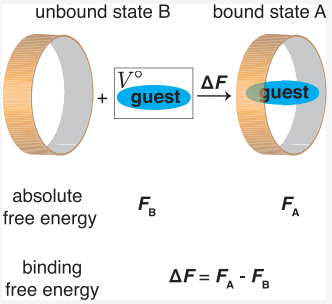

Noncovalent molecular binding is essential for many processes such as self-assembly[1] and signal transduction.[2] Accurate estimation of the absolute binding affinity could provide insight into the physicochemical interactions that drive these processes.[3] Computing binding free energy also has important practical applications in drug discovery for *in silico* screening and design of small molecules that bind with a target protein.[4]

Numerous methods have been introduced for computing binding free energy. The alchemical double decoupling (ADD)[5] and the potential of mean force (PMF) methods[6,7] are both exact. They rely on extensive molecular dynamics simulations and can, in principle, produce values directly comparable to experimental measurements, barring the approximations introduced in force field parametrization. Notably, these two methods require simulations for both the two end states (bound and unbound) and many alchemical/physical intermediate states that bridge them.[5−7] In addition to increasing the computational cost significantly, intermediate states are nontrivial to construct, and their definition varies greatly among systems. On the other hand, the molecular mechanics/Poisson−Boltzmann or generalized Born and surface area continuum solvation (MM/PBSA[8] or MM/GBSA[9]) methods circumvent the need for intermediate states and require only sampling from the two end states. While computationally more efficient, MM/GBSA and MM/PBSA are less accurate due to the approximations introduced for estimating the entropic contributions.[8,9] The quality of such approximations is system dependent, and their impact on the computed free energy values is hard to gauge *a priori*.

In this Letter, we introduce a new method, DeepBAR, to compute the binding free energy as the difference of the absolute free energy for the bound state A and the unbound state B, i.e., $\Delta F_{\text{binding}} = F_A - F_B$. Previously, we showed that absolute free energy could be calculated using deep generative models and the Bennett acceptance ratio (BAR) method with high accuracy.[10] Like MM/GBSA and MM/PBSA, DeepBAR requires sampling only from the end states. A crucial difference from these methods is that DeepBAR is exact and can achieve the same accuracy as ADD and PMF. Therefore, it is designed to perform fast and accurate computations of binding free energy.

We first briefly review the method for calculating absolute free energy using reference states constructed with deep generative models.[10] For conciseness in notation, we present the algorithmic details using state A as an example, but the procedure applies to state B equally. We define the reference state A° as a probabilistic model, $q_{A^\circ}(\boldsymbol{x};\boldsymbol{\theta})$, and its energy function as $U_{A^\circ}(\boldsymbol{x}) = -\beta^{-1} \log q_{A^\circ}(\boldsymbol{x};\boldsymbol{\theta})$, where $\boldsymbol{x}$ represents the Cartesian coordinates of a molecular configuration and $\boldsymbol{\theta}$ corresponds to the model parameters. $\beta = 1/(k_B T)$ is the inverse of the product of the Boltzmann constant (k_B) and temperature (T). The benefit of defining the reference state as a probabilistic model is that because $q_{A^\circ}(\boldsymbol{x};\boldsymbol{\theta})$ is normalized, the absolute free energy of this state is 0, i.e.,

$$F_{A^\circ} = -\beta^{-1} \log \int e^{-\beta U_{A^\circ}(\boldsymbol{x})}\, d\boldsymbol{x} = -\beta^{-1} \log \int q_{A^\circ}(\boldsymbol{x};\boldsymbol{\theta})\, d\boldsymbol{x} = 0 \quad (1)$$

Received: January 19, 2021
Accepted: February 25, 2021

https://dx.doi.org/10.1021/acs.jpclett.1c00189
J. Phys. Chem. Lett. 2021, 12, 2509−2515

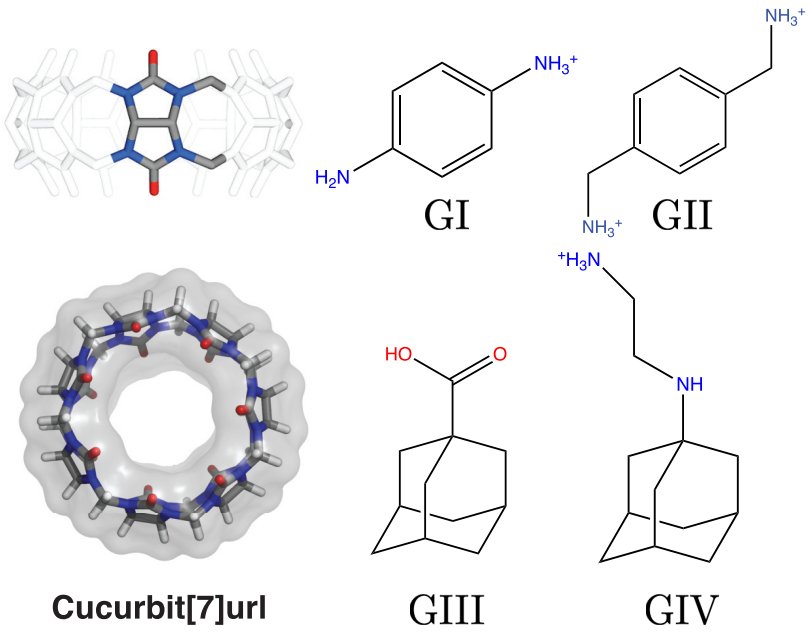

Figure 1. Illustration of the cucurbit[7]uril (CB7) host−guest system used for testing the DeepBAR method. The left two panels provide a side and top view of the host, with its periodic unit highlighted in the top panel. Structures of the four guests (GI−GIV) are shown in the right panels.

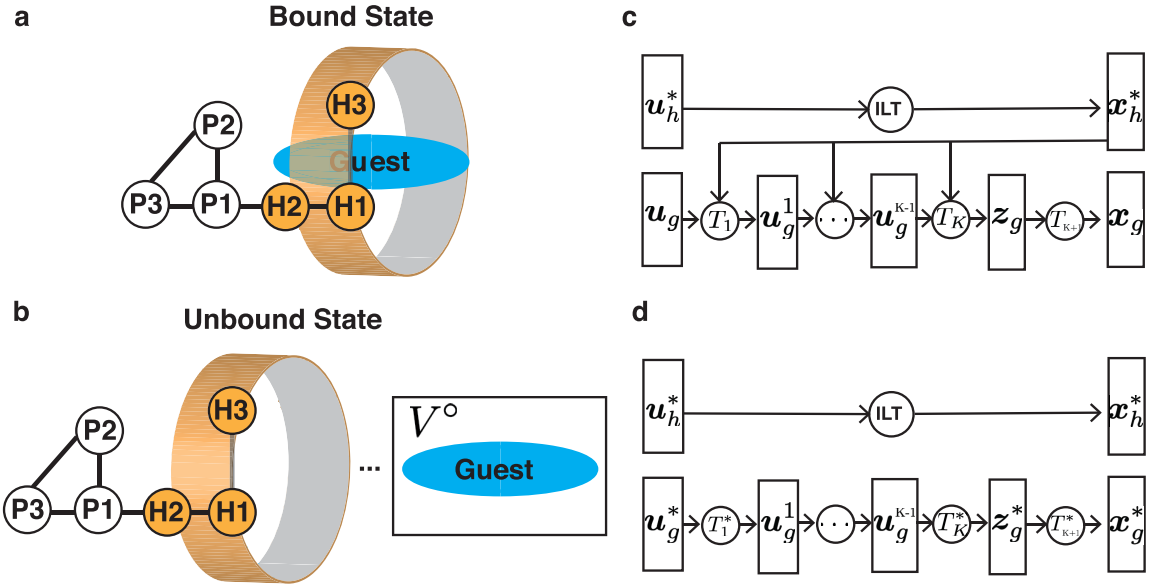

Figure 2. Parameterizing reference states with deep generative models using samples collected with restrained molecular dynamics simulations. (a, b) Illustration of the fixed anchor particles (P1, P2, and P3) and virtual sites (H1, H2, and H3) used to restrain the host in both bound and unbound states and guest molecules in the unbound state. Detailed definitions for these anchor particles and virtual sites are provided in the Supporting Information. (c, d) The flow-based deep generative models used for parametrizing reference state A° (c) and B° (d). The Cartesian coordinates for the host ($\boldsymbol{x}_h^*$) and guest ($\boldsymbol{x}_g/\boldsymbol{x}_g^*$) are determined from normal random variables ($\boldsymbol{u}_h^*$) via invertible linear transformations (ILT) and from multiple bijective transformations of uniformly distributed random variables ($\boldsymbol{u}_g/\boldsymbol{u}_g^*$), respectively.

Therefore, the absolute free energy for state A equals to its free energy difference from A°, $\Delta F_{A^\circ\to A}$, and can be determined by solving the BAR equation:[11]

$$\sum_{n=1}^{N_{A^\circ}} f(\beta[\Delta U(\boldsymbol{x}_{A^\circ}^n) - M - \Delta F_{A^\circ\to A}]) = \sum_{n=1}^{N_A} f(-\beta[\Delta U(\boldsymbol{x}_A^n) - M - \Delta F_{A^\circ\to A}]) \quad (2)$$

where $f(t) = 1/(1 + e^t)$, $\Delta U(\boldsymbol{x}) = U_A(\boldsymbol{x}) - U_{A^\circ}(\boldsymbol{x})$, and $M = \log(N_A/N_{A^\circ})$. A reliable estimation of the free energy difference, $\Delta F_{A^\circ\to A}$, from the above equation requires (*i*) independent samples $\{\boldsymbol{x}_{A^\circ}^n: n = 1, \cdots, N_{A^\circ}\}$ from the reference state A° besides state A samples $\{\boldsymbol{x}_A^n: n = 1, \cdots, N_A\}$ that can be produced using molecular dynamics simulations and (*ii*) a significant phase space overlap between states A° and A. Both requirements can be satisfied if $q_{A^\circ}(\boldsymbol{x};\boldsymbol{\theta})$ is designed as deep generative models, a special class of probabilistic models, with parameters ($\boldsymbol{\theta}$) that maximize the log-likelihood on samples $\{\boldsymbol{x}_A^n, n = 1, \cdots, N_A\}$ generated from state A. Deep generative models allow precise

https://dx.doi.org/10.1021/acs.jpclett.1c00189
J. Phys. Chem. Lett. 2021, 12, 2509−2515

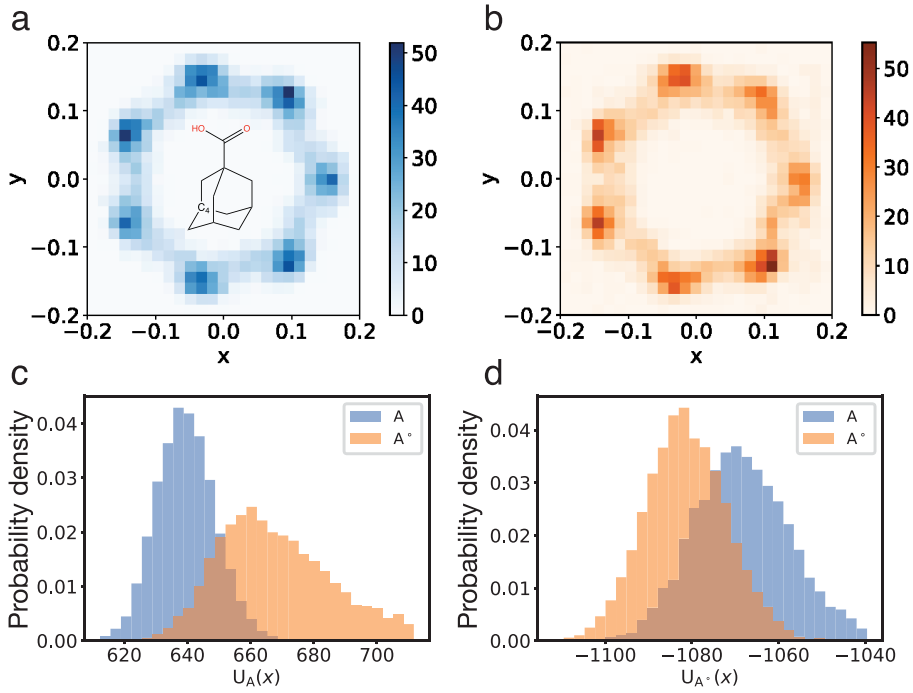

Figure 3. Phase space overlap between state A and A° for the CB7-GIII host−guest system. (a, b) Probability distribution of the $x-y$ coordinates of atom C_4 on guest GIII for state A (a) and A° (b). Atom C_4 is one of the three spiro carbon atoms connecting the two rings, as shown in the embedded structure in part a. (c, d) Distributions of the value (in kcal/mol) of energy functions U_A (c) and $U_{A°}$ (d) on samples from state A (blue) and state A° (orange).

evaluation of the absolute probability for any molecular configuration and for generating independent configurations at negligible computational cost. Log-likelihood maximization further ensures the similarity between configurations from deep generative models and those produced by molecular dynamics simulations for state A.

To demonstrate the efficacy of DeepBAR for computing binding free energy, we applied it to four host−guest systems (Figure 1).[12] These systems are small in size and permit exhaustive conformational sampling. They are widely used for benchmarking free energy calculation methods.[13] The host molecule, cucurbit[7]uril (CB7),[14−17] is an achiral ring consisting of seven glycoluril monomers. It features high binding affinities, especially for guests with a hydrophobic core that can fit tightly into its nonpolar binding pocket. To further simplify the system and eliminate sampling issues that might come from explicit water molecules, we used the OBC implicit solvent model[18] in calculating the binding free energy.

Molecular dynamics simulations were performed to collect sample configurations from state A and B. We removed the translational and rotational degrees of freedom for the host in state A and from both the host and the guest in state B using restraining potentials. These potentials were defined with the use of fixed anchor particles (P1, P2, and P3) and virtual sites (H1, H2, and H3) of the host (Figures 2a and 2b). As detailed in the Supporting Information (SI), removing these degrees of freedom does not impact the accuracy of free energy calculations but facilitates conformational sampling. For notational purposes, we use $\boldsymbol{x}_h$ and $\boldsymbol{x}_g$ for the full phase space of host and guest and $\boldsymbol{x}_h^*$ and $\boldsymbol{x}_g^*$ for the ones with translational and rotational degrees of freedom removed.

Host−guest conformations from MD simulations were used to learn references states A° as $q_{A°}(\boldsymbol{x}_h^*,\boldsymbol{x}_g)$ and B° as $q_{B°}(\boldsymbol{x}_h^*,\boldsymbol{x}_g^*)$ using flow-based generative models.[19−22] Flow-based models produce molecular configurations by applying a series of bijective transformations to independent random variables that have normal or uniform distributions (Figures 2c and 2d). The transformations are often represented as neural networks to ensure the expressibility of the probabilistic models so that they can approximate the complex distributions from MD simulations well. Because random variable generation from both normal and uniform distributions is trivial to perform, sampling molecular configurations by applying transformations to these random samples is straightforward and computationally efficient. In contrast to MD simulations that provide only the relative probability for molecular configurations due to the unknown partition function, flow-based models compute the absolute configurational probability by reweighting the probability of normal/uniform random variables with appropriate Jacobians. More details on the flow-based generative models are provided in the Supporting Information. The probability distribution for guest molecules in state A is dependent on the conformation of the host, and we decomposed the joint probability distribution as $q_{A°}(\boldsymbol{x}_h^*,\boldsymbol{x}_g) = q_{A°}(\boldsymbol{x}_h^*) \times q_{A°}(\boldsymbol{x}_g|\boldsymbol{x}_h^*)$. On the other hand, the host and guest are independent from each other in state B, and correspondingly, we decomposed the joint probability distribution as $q_{B°}(\boldsymbol{x}_h^*,\boldsymbol{x}_g^*) = q_{B°}(\boldsymbol{x}_h^*) \times q_{B°}(\boldsymbol{x}_g^*)$.

After learning the reference states, we first evaluated their phase space overlap with the target states using marginal distributions of specific degrees of freedom. These marginal distributions can be estimated using sample configurations from reference and target states. Samples from the reference state were generated from the trained bijective transformations of random variables. Figures 3a and 3b show the distributions of $x-y$ coordinates of atom C_4 on guest GIII for state A and state A°, respectively. Results for other systems and states are provided in Figures S1−S6. Because the host CB7 has a 7-fold rotational symmetry and its middle section plane is aligned with

https://dx.doi.org/10.1021/acs.jpclett.1c00189
J. Phys. Chem. Lett. 2021, 12, 2509−2515

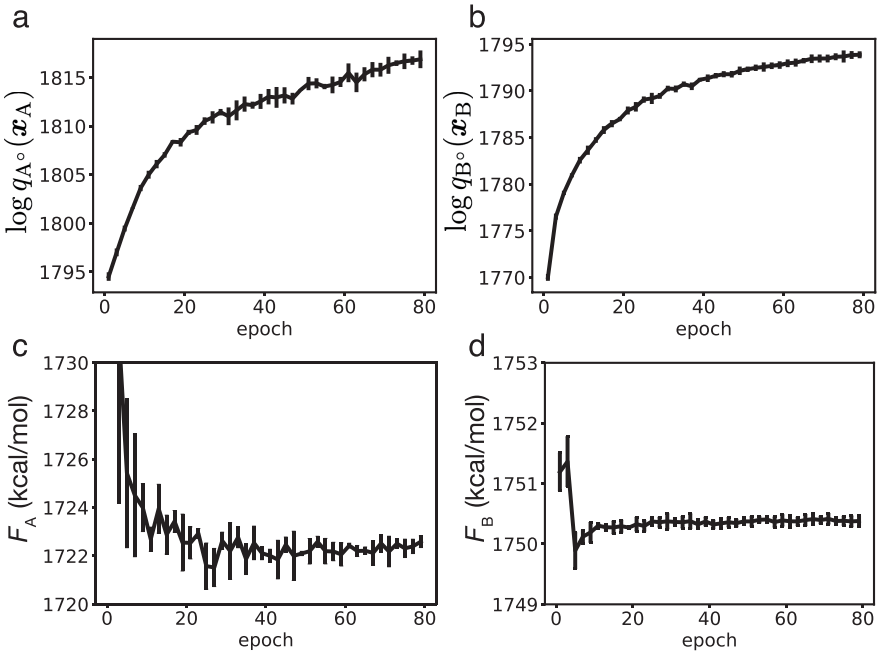

Figure 4. Free energy values estimated with DeepBAR are robust with respect to model quality. (a, b) Log-likelihood of the generative models for state A° (a) and B° (b) on training data as a function of the number of epochs used for model parametrization. (c, d) Values of the absolute free energy for state A (c) and B (d) calculated using models trained with different numbers of epochs.

the $x-y$ plane, the distribution of C_4 atom's $x-y$ coordinates in state A has a 7-fold rotational symmetry too (Figure 3a). Figure 3b shows that the corresponding distribution from the learned reference state A° matches quite well with that from state A even though the distribution has multiple modes. Figures S5a−S5d show similar agreement for the distributions of two representative dihedral angles between state A and A° for guest GIII.

In addition to the marginal distributions, we further examined the 3D conformations produced by generative models directly. The potential energy functions of the target states serve as a metric for the quality of these conformations as unphysical structures, and even clashes between atoms will lead to high energy values. Figure 3c shows the probability distributions of the energy function U_A computed using sample configurations from state A (blue) and A° (orange) for the host−guest system with GIII. There is a significant overlap between the two distributions, supporting the ability of generative models in producing realistic molecular configurations with reasonable energy. In addition to the distributions of the target state energy function, we also computed and compared the distributions of the reference energy function U_{A° (Figure 3d). Because the reference state was trained to maximize its likelihood on samples from state A, its energy function $U_{A^\circ}(\boldsymbol{x})$ has similar values on samples from itself and from state A. Correspondingly, the overlap between the two distributions for $U_{A^\circ}(\boldsymbol{x})$ is more significant than those for $U_A(\boldsymbol{x})$. The corresponding results for state B and B° are provided in Figures S5e and S5f and support similar conclusions. Similar overlaps are also observed for all other guest molecules (Figures S7−S9).

The significant phase space overlap between reference and target states allows robust estimation of their free energy difference with the BAR equation (eq 2). Notably, for both state A and B, the estimations are relatively independent of the quality of the generative models. As shown in Figure 4c and 4d, the absolute free energy, F_A and F_B, converges by about 50 epochs of training, even though the generative models at this stage are less optimal and have smaller likelihood on the sample configurations from MD simulations (Figure 4a and 4b) compared to the final ones (80 epochs of training) that are used for making Figure 3. Similar results hold for all other guests, too (Figures S10−S12). Therefore, the free energy estimation is not very demanding on the phase space overlap between reference and target states and does not require the deep generative models to perfectly reproduce the probability distributions of target states.

With the absolute free energy of states A and B calculated, we can compute the binding free energy as their difference, i.e., $\Delta F_{binding} = F_A - F_B$ (Table 1). For comparison, we also computed the binding free energy of the four guest molecules using the PMF method.[6,7] In contrast to DeepBAR, PMF requires MD simulations for both end states and intermediate states in which the guest molecule is placed at increasing distances from the host. These intermediate states help bridge the two end states that do not have phase space overlap. They must be introduced at a slow pace to ensure sufficient overlap between any two adjacent states as well. For all four guests, we found that 95 intermediate states, corresponding to 97 windows in Table 2, are sufficient to produce converged results. There are significant overlaps between the probability distributions of

Table 1. Absolute Free Energy of States A and B, F_A and F_B, and Binding Free Energy $\Delta F_{binding}$[a] of the Four Guests Calculated Using the DeepBAR Method

guest	F_A	F_B	$\Delta F_{binding}$
GI	1554.73 ± 0.29	1567.37 ± 0.22	−12.63 ± 0.25
GII	1649.22 ± 0.12	1664.05 ± 0.18	−14.82 ± 0.28
GIII	1722.73 ± 0.17	1750.38 ± 0.17	−27.65 ± 0.15
GIV	1750.68 ± 0.20	1780.54 ± 0.24	−29.87 ± 0.21

[a]Standard deviations are computed using three independent repeats and the unit of free energy is kcal/mol.

https://dx.doi.org/10.1021/acs.jpclett.1c00189
J. Phys. Chem. Lett. 2021, 12, 2509−2515

Table 2. Comparison of Binding Free Energy $\Delta F_{binding}$[a] of the Four Guests Calculated Using the DeepBAR Method, the PMF-based Method, and the MM/GBSA Method

		PMF			
guest	DeepBAR	97 windows[b]	49 windows	33 windows	MM/GBSA
GI	−12.63 ± 0.25	−12.76 ± 0.27	−12.74 ± 0.42	−13.47 ± 1.83	−3.97 ± 0.19
GII	−14.82 ± 0.28	−15.29 ± 0.09	−14.90 ± 0.47	−14.69 ± 4.64	−6.53 ± 0.15
GIII	−27.65 ± 0.15	−27.57 ± 0.13	−27.32 ± 0.60	−26.81 ± 0.80	−20.61 ± 0.16
GIV	−29.87 ± 0.21	−30.61 ± 0.32	−31.26 ± 0.64	−29.26 ± 0.67	−22.65 ± 0.14

[a]Standard deviations are computed using three independent repeats and the unit of free energy is kcal/mol. [b]The PMF method with n windows means it samples from 2 end states and $n - 2$ intermediate states.

collective variables for adjacent states (Figures S13−S24), and the computed binding free energy from three independent repeats shows small standard deviations (Table 2). We also computed the binding free energy using PMF with 49 and 33 windows. These results have much higher uncertainty. The binding free energy calculated using DeepBAR agrees well with that from PMF with 97 windows and reaches a similar statistical uncertainty level. The values are also comparable to results from prior studies.[23] On the other hand, the results computed using MM/GBSA show large systematic errors. Since 97 and 2 independent MD simulations are needed for the two methods, DeepBAR is almost 50 times more efficient than PMF in terms of the amount of sampling required to reach the same results with similar statistical uncertainty.

In summary, DeepBAR is exact and can accurately compute binding free energy using only a small fraction of the computational resource required by PMF. It does not suffer from the approximations that are inherent in other end state methods such as MM/GBSA and MM/PBSA.[8,9] Although we benchmarked the method using host−guest systems, it can be readily applied to compute protein−ligand and protein−protein binding free energy.

We note that GB implicit solvent simulations[18] were used to sample molecular configurations and parametrize deep generative models. Because explicit solvent simulations often provide better agreement with experiments for free energy calculations, it is desirable to couple them with the DeepBAR method. However, there can be challenges in modeling the ensemble distribution of all degrees of freedom in an explicit solvent system with generative models. Including solvent molecules dramatically increases the system size and introduces permutational symmetry (permutation of water molecules does not change the system's energy) to the ensemble distribution. Encouraging progress is being made in designing flow-based generative models for systems with large sizes and permutational symmetry.[22,24−26] Combining these techniques with DeepBAR will be an exciting future direction.

COMPUTATIONAL METHODS

MD simulations were used for conformational sampling in both DeepBAR and PMF. A cutoff distance of 1.4 nm was used for nonbonded interactions including both electrostatic and van der Waals interactions. The temperature of the simulations was maintained at 298 K using the Langevin dynamics with a friction coefficient of 1 ps^{-1}. The time step was set to 1 fs. For guest molecules GI, GII, and GIII, 20 ns of simulations were performed and conformations were saved at every 0.1 ps. Because the guest GIV has a larger size and is slower to rotate inside the host, we used 100 ns of simulations to sample and collected conformations at every 0.5 ps. Therefore, 200000 conformations were produced for all four guests to train generative models and reference states.

Invertible linear transformations (ILT) were used to model the transformation between $\boldsymbol{u}_h^*$ and $\boldsymbol{x}_h^*$ for both state A and state B, i.e., $\boldsymbol{x}_h^* = \mathbf{M}\boldsymbol{u}_h^* + \boldsymbol{\mu}$, where $\mathbf{M}$ is an invertible matrix. Rational quadratic neural spline flows[21] (RQ-NSF) with 20 coupling layers, each of which has 32 hidden units, were used to model the transformation between $\boldsymbol{u}_g^*$ and $\boldsymbol{z}_g^*$ for state B and between $\boldsymbol{u}_g|\boldsymbol{x}_h^*$ and $\boldsymbol{z}_g$ for state A. The architectures of the RQ-NSF are the same as that used and also described in detail in our previous study.[10] The 200000 conformations sampled from state A (or B) were split into two sets, each of which has 100000 conformations, where 90000 configurations of the first set were used as the training data for learning RQ-NSF for state A° (or B°) and the remaining 10000 conformations were used as validation data. The 100000 conformations from the second set were used as $\boldsymbol{x}_A$ (or $\boldsymbol{x}_B$) in computing $\Delta F_{A^\circ\to A}$ (or $\Delta F_{B^\circ\to B}$) using eq 2. The stochastic gradient descent method, Adam optimizer,[27] was used to optimize the RQ-NSF models by maximizing its likelihood on the training data. The learning rate was set to 0.001, and the training batch size was 512. After each epoch of training, the likelihood of the RQ-NSF model on the validation data was calculated and the training of the RQ-NSF model stopped when its likelihood on the validation data started to decrease, i.e., when the RQ-NSF model started to overfit. After learning, 100000 conformations were sampled from state A° (or B°), and these conformations were used as $\boldsymbol{x}_{A^\circ}$ (or $\boldsymbol{x}_{B^\circ}$) in computing $\Delta F_{A^\circ\to A}$ (or $\Delta F_{B^\circ\to B}$) by solving the BAR equation (eq 2) using the FastMBAR solver.[28]

The PMF method used in this study follows the attach-pull-release (APR) framework presented in ref 7 for computing host−guest binding free energy. In this framework, the intermediate states are designed to open the host cavity and to remove guest and release host restraints in the three attachment, pulling, and release phases. Detailed information about restraint potentials used in the intermediate states is included in the Supporting Information. After sampling from both intermediate states and end states, the binding free energy was calculated by solving the multistate Bennett acceptance ratio equation.[29]

The MM/GBSA calculations were conducted using the MMPBSA.py program[30] with the solute entropy calculated using the normal-mode analysis (Table S1).

ASSOCIATED CONTENT

Supporting Information

The Supporting Information is available free of charge at https://pubs.acs.org/doi/10.1021/acs.jpclett.1c00189.

Definition of bound and unbound states, simulation details for bound and unbound states, generative models for reference state construction, bijective transformations

https://dx.doi.org/10.1021/acs.jpclett.1c00189
J. Phys. Chem. Lett. 2021, 12, 2509−2515

between Cartesian and internal coordinates, details on PMF calculations, (Figure S1) the specific atoms and dihedral angles of guest molecules, (Figures S2) illustration of the RQ-NSF layer used to define the bijective transformations, (Figures S3−S6) overlap of marginal distributions of specific degrees of freedom between state A/B and state A°/B°, (Figures S7−S9) energy function distribution overlap between state A/B and state A°/B°, (Figures S10−S12) log-likelihood of the generative model on training data and calculated absolute free energy, (Figures S13−S24) overlaps between distributions of collective variables for adjacent states in PMF, (Figure S25) illustration of the fixed anchor particles (P1, P2, and P3) and virtual sites (H1, H2, and H3) introduced for restraining the host's position and orientation, (Figure S26) the definition of the virtual site H4 of the host used for constructing biasing potentials to enlarge the host cavity portal, (Figure S27) illustration of the collective variables introduced to restrain the position and orientation of guest molecules, and (Table S1) the enthalpy and entropy changes calculated using MM/GBSA for binding free energy (PDF)

AUTHOR INFORMATION

Corresponding Author

Bin Zhang − *Department of Chemistry, Massachusetts Institute of Technology, Cambridge, Massachusetts 02139, United States;* orcid.org/0000-0002-3685-7503; Email: binz@mit.edu

Author

Xinqiang Ding − *Department of Chemistry, Massachusetts Institute of Technology, Cambridge, Massachusetts 02139, United States;* orcid.org/0000-0002-4598-8732

Complete contact information is available at: https://pubs.acs.org/10.1021/acs.jpclett.1c00189

Notes

The authors declare no competing financial interest.

ACKNOWLEDGMENTS

This work was supported by the National Institutes of Health (1R35GM133580).

REFERENCES

(1) Bowden, N.; Terfort, A.; Carbeck, J.; Whitesides, G. M. Self-Assembly of Mesoscale Objects into Ordered Two-Dimensional Arrays. *Science* **1997**, *276*, 233−235.

(2) Murcko, M. A. Computational Methods to Predict Binding Free Energy in Ligand-Receptor Complexes. *J. Med. Chem.* **1995**, *38*, 4953−4967.

(3) Gohlke, H.; Kiel, C.; Case, D. A. Insights into Protein−Protein Binding by Binding Free Energy Calculation and Free Energy Decomposition for the Ras−Raf and Ras−RalGDS Complexes. *J. Mol. Biol.* **2003**, *330*, 891−913.

(4) Jorgensen, W. L. The many roles of computation in drug discovery. *Science* **2004**, *303*, 1813−1818.

(5) Boresch, S.; Tettinger, F.; Leitgeb, M.; Karplus, M. Absolute Binding Free Energies: A Quantitative Approach for Their Calculation. *J. Phys. Chem. B* **2003**, *107*, 9535−9551.

(6) Woo, H.-J.; Roux, B. Calculation of absolute protein−ligand binding free energy from computer simulations. *Proc. Natl. Acad. Sci. U. S. A.* **2005**, *102*, 6825−6830.

(7) Henriksen, N. M.; Fenley, A. T.; Gilson, M. K. Computational Calorimetry: High-Precision Calculation of Host−Guest Binding Thermodynamics. *J. Chem. Theory Comput.* **2015**, *11*, 4377−4394.

(8) Massova, I.; Kollman, P. A. Combined molecular mechanical and continuum solvent approach (MM-PBSA/GBSA) to predict ligand binding. *Perspect. Drug Discovery Des.* **2000**, *18*, 113−135.

(9) Genheden, S.; Ryde, U. The MM/PBSA and MM/GBSA methods to estimate ligand-binding affinities. *Expert Opin. Drug Discovery* **2015**, *10*, 449−461.

(10) Ding, X.; Zhang, B. Computing Absolute Free Energy with Deep Generative Models. *J. Phys. Chem. B* **2020**, *124*, 10166−10172.

(11) Bennett, C. H. Efficient estimation of free energy differences from Monte Carlo data. *J. Comput. Phys.* **1976**, *22*, 245−268.

(12) Mobley, D. L.; Gilson, M. K. Predicting Binding Free Energies: Frontiers and Benchmarks. *Annu. Rev. Biophys.* **2017**, *46*, 531−558.

(13) Rizzi, A.; Jensen, T.; Slochower, D. R.; Aldeghi, M.; Gapsys, V.; Ntekoumes, D.; Bosisio, S.; Papadourakis, M.; Henriksen, N. M.; de Groot, B. L.; et al. The SAMPL6 SAMPLing challenge: assessing the reliability and efficiency of binding free energy calculations. *J. Comput.-Aided Mol. Des.* **2020**, *34*, 601−633.

(14) Cao, L.; Šekutor, M.; Zavalij, P. Y.; Mlinarić-Majerski, K.; Glaser, R.; Isaacs, L. Cucurbit[7] uril · Guest Pair with an Attomolar Dissociation Constant. *Angew. Chem., Int. Ed.* **2014**, *53*, 988−993.

(15) Liu, S.; Ruspic, C.; Mukhopadhyay, P.; Chakrabarti, S.; Zavalij, P. Y.; Isaacs, L. The Cucurbit[n] uril Family: Prime Components for Self-Sorting Systems. *J. Am. Chem. Soc.* **2005**, *127*, 15959−15967.

(16) Moghaddam, S.; Inoue, Y.; Gilson, M. K. Host-Guest Complexes with Protein-Ligand-like Affinities: Computational Analysis and Design. *J. Am. Chem. Soc.* **2009**, *131*, 4012−4021.

(17) Rekharsky, M. V.; Mori, T.; Yang, C.; Ko, Y. H.; Selvapalam, N.; Kim, H.; Sobransingh, D.; Kaifer, A. E.; Liu, S.; Isaacs, L.; et al. A synthetic host-guest system achieves avidin-biotin affinity by overcoming enthalpy−entropy compensation. *Proc. Natl. Acad. Sci. U. S. A.* **2007**, *104*, 20737−20742.

(18) Onufriev, A.; Bashford, D.; Case, D. A. Exploring protein native states and large-scale conformational changes with a modified generalized born model. *Proteins: Struct., Funct., Genet.* **2004**, *55*, 383−394.

(19) Rezende, D. J.; Mohamed, S. Variational Inference with Normalizing Flows. In *Proceedings of the 32nd International Conference on Machine Learning*; ICML, Lille, France, 6−11 July 2015; pp 1530−1538.

(20) Dinh, L.; Sohl-Dickstein, J.; Bengio, S. Density Estimation Using Real NVP. In *Proceedings of the 5th International Conference on Learning Representations*; ICLR, Toulon, France, 24−26 April 2017, Conference Track Proceedings.

(21) Durkan, C.; Bekasov, A.; Murray, I.; Papamakarios, G. In *Advances in Neural Information Processing Systems 32*; Wallach, H., Larochelle, H., Beygelzimer, A., d' Alché-Buc, F., Fox, E., Garnett, R., Eds.; Curran Associates, Inc.: 2019; pp 7511−7522.

(22) Noé, F.; Olsson, S.; Köhler, J.; Wu, H. Boltzmann generators: Sampling equilibrium states of many-body systems with deep learning. *Science* **2019**, *365*, No. eaaw1147.

(23) Yin, J.; Fenley, A. T.; Henriksen, N. M.; Gilson, M. K. Toward Improved Force-Field Accuracy through Sensitivity Analysis of Host-Guest Binding Thermodynamics. *J. Phys. Chem. B* **2015**, *119*, 10145−10155.

(24) Wirnsberger, P.; Ballard, A. J.; Papamakarios, G.; Abercrombie, S.; Racanière, S.; Pritzel, A.; Jimenez Rezende, D.; Blundell, C. Targeted free energy estimation via learned mappings. *J. Chem. Phys.* **2020**, *153*, 144112.

(25) Bender, C. M.; Garcia, J. J.; O'Connor, K.; Oliva, J. Permutation invariant likelihoods and equivariant transformations. *arXiv (Computer Science, Machine Learning)*, February 5, 2019, 1902.0196, ver. 1. https://arxiv.org/abs/1902.01967v1.

(26) Köhler, J.; Klein, L.; Noé, F. Equivariant flows: sampling configurations for multi-body systems with symmetric energies. *arXiv (Statistics, Machine Learning)*, October 2, 2019, 1910.00753, ver. 1. https://arxiv.org/abs/1910.00753.

(27) Kingma, D. P.; Ba, J. Adam: A Method for Stochastic Optimization. In *Proceedings of the 3rd International Conference on Learning Representations*; ICLR: San Diego, CA, USA, 7−9 May 2015, Conference Track Proceedings.
(28) Ding, X.; Vilseck, J. Z.; Brooks, C. L. Fast Solver for Large Scale Multistate Bennett Acceptance Ratio Equations. *J. Chem. Theory Comput.* **2019**, *15*, 799−802.
(29) Shirts, M. R.; Chodera, J. D. Statistically optimal analysis of samples from multiple equilibrium states. *J. Chem. Phys.* **2008**, *129*, 124105.
(30) Miller, B. R.; McGee, T. D.; Swails, J. M.; Homeyer, N.; Gohlke, H.; Roitberg, A. E. MMPBSA.py: An Efficient Program for End-State Free Energy Calculations. *J. Chem. Theory Comput.* **2012**, *8*, 3314−3321.

https://dx.doi.org/10.1021/acs.jpclett.1c00189
J. Phys. Chem. Lett. 2021, 12, 2509−2515